Research Article | Vol. 25, No. 23 | 13 Nov 2017 | OPTICS EXPRESS 29161

Optics EXPRESS

Simultaneous fluorescence and surface charge measurements on organic semiconductor-coated silica microspheres in (non)polar liquids

R. GROLLMAN, G. FOUNDS, R. WALLACE, AND O. OSTROVERKHOVA*

Department of Physics, Oregon State University, Corvallis, OR 97331, USA
**oksana@science.oregonstate.edu*

Abstract: We present an experimental platform which combines spectroscopic capabilities with time-resolved measurements of effective surface charge at solid-liquid interfaces. Silica microspheres, pristine and coated with various organic semiconductor molecules, were optically trapped either in water or in toluene. Adsorption of organic semiconductor molecules on the microspheres was observed via appearance of fluorescence and dramatic reduction in the effective surface charge, measured concurrently on individual spheres, with elementary charge resolution. The versatile platform accommodates possibilities to study a variety of photoinduced processes simultaneously with measurements of surface charge and can be incorporated in devices such as microreactors and microfluidics.

OCIS codes: (120.0120) Instrumentation, measurement, and metrology; (160.4890) Organic materials; (180.2520) Fluorescence microscopy; (240.6700) Surfaces.

References and links

1. F. Zaera, "Probing Liquid/Solid Interfaces at the Molecular Level," Chem. Rev. **112**(5), 2920–2986 (2012).
2. G. Seth Roberts, T. A. Wood, W. J. Frith, and P. Bartlett, "Direct measurement of the effective charge in nonpolar suspensions by optical tracking of single particles," J. Chem. Phys. **126**(19), 194503 (2007).
3. G. Pesce, V. Lisbino, G. Rusciano, A. Sasso, and C. U. Monte, "Optical manipulation of charged microparticles in polar fluids," Electrophoresis **34**(22-23), 3141–3149 (2013).
4. F. Strubbe, F. Beunis, and K. Neyts, "Detection of Elementary Charges on Colloidal Particles," Phys. Rev. Lett. **100**(21), 218301 (2008).
5. F. Beunis, F. Strubbe, K. Neyts, and D. Petrov, "Beyond Millikan: The dynamics of charging events on individual colloidal particles," Phys. Rev. Lett. **108**(1), 016101 (2012).
6. M. Gacek, D. Bergsman, E. Michor, and J. C. Berg, "Effects of Trace Water on Charging of Silica Particles Dispersed in a Nonpolar Medium," Langmuir **28**(31), 11633–11638 (2012).
7. G. N. Smith, J. E. Hallett, J. Eastoe, and G. N. Smith, "Soft Matter Celebrating Soft Matter's 10th Anniversary: Influencing the charge of poly(methyl methacrylate) latexes in nonpolar solvents," Soft Matter **11**(41), 8029–8041 (2015).
8. J. Lee, Z. L. Zhou, and S. H. Behrens, "Charging Mechanism for Polymer Particles in Nonpolar Surfactant Solutions: Influence of Polymer Type and Surface Functionality," Langmuir **32**(19), 4827–4836 (2016).
9. A. Nakao and M. Fujiki, "Visualizing spontaneous physisorption of non-charged conjugated polymers onto neutral surfaces of spherical silica in nonpolar solvents," Polym. J. **47**, 434–442 (2015).
10. T. S. Mahadevan and S. H. Garofalini, "Dissociative chemisorption of water onto silica surfaces and formation of hydronium ions," J. Phys. Chem. C **112**, 1507–1515 (2008).
11. A. Steinbach, T. Paust, M. Pluntke, O. Marti, and D. Volkmer, "Selective Adsorption of Functionalized Nanoparticles to Patterned Polymer Brush Surfaces and Its Probing with an Optical Trap," ChemPhysChem **14**(15), 3523–3531 (2013).
12. T. A. Wood, G. S. Roberts, S. Eaimkhong, and P. Bartlett, "Characterization of microparticles with driven optical tweezers," Faraday Discuss. **137**, 319–333 (2008).
13. E. M. Peterson and J. M. Harris, "Imaging Fluorescent Nanoparticles To Probe Photoinduced Charging of a Semiconductor-Solution Interface," Langmuir **29**(38), 11941–11949 (2013).
14. G. Pesce, G. Rusciano, G. Zito, and A. Sasso, "Simultaneous measurements of electrophoretic and dielectrophoretic forces using optical tweezers," Opt. Express **23**(7), 9363–9368 (2015).
15. G. Pesce, B. Mandracchia, E. Orabona, G. Rusciano, L. De Stefano, and A. Sasso, "Mapping electric fields generated by microelectrodes using optically trapped charged microspheres," Lab Chip **11**(23), 4113–4116 (2011).
16. H. Park and T. W. LeBrun, "Contact Electrification of Individual Dielectric Microparticles Measured by Optical

#307553 https://doi.org/10.1364/OE.25.029161
Journal © 2017 Received 20 Sep 2017; revised 31 Oct 2017; accepted 31 Oct 2017; published 8 Nov 2017

Optics EXPRESS

Tweezers in Air," ACS Appl. Mater. Interfaces **8**(50), 34904–34913 (2016).
17. O. Ostroverkhova, "Organic optoelectronic materials : mechanisms and applications," Chem. Rev. **116**(22), 13279–13412 (2016).
18. A. Platt, M. Kendrick, M. Loth, J. Anthony, and O. Ostroverkhova, "Temperature dependence of exciton and charge carrier dynamics in organic thin films," Phys. Rev. B **84**, 235209 (2011).
19. W. E. B. Shepherd, A. D. Platt, M. J. Kendrick, M. A. Loth, J. E. Anthony, and O. Ostroverkhova, "Energy transfer and exciplex formation and their impact on exciton and charge carrier dynamics in organic films," J. Phys. Chem. Lett. **2**, 362–366 (2011).
20. M. J. Kendrick, A. Neunzert, M. M. Payne, B. Purushothaman, B. D. Rose, J. E. Anthony, M. M. Haley, and O. Ostroverkhova, "Formation of the donor-acceptor charge-transfer exciton and its contribution to charge photogeneration and recombination in small-molecule bulk heterojunctions," J. Phys. Chem. C **116**, 18108–18116 (2012).
21. W. E. B. Shepherd, R. Grollman, A. Robertson, K. Paudel, R. Hallani, M. Loth, J. E. Anthony, and O. Ostroverkhova, "Single-molecule imaging of organic semiconductors: Toward nanoscale insights into photophysics and molecular packing," Chem. Phys. Lett. **629**, 29–35 (2015).
22. R. J. Kline, S. D. Hudson, X. Zhang, D. J. Gundlach, A. J. Moad, O. D. Jurchescu, T. N. Jackson, S. Subramanian, J. E. Anthony, M. F. Toney, and L. J. Richter, "Controlling the microstructure of solution-processable small molecules in thin-film transistors through substrate chemistry," Chem. Mater. **23**, 1194–1203 (2011).
23. W. E. B. Shepherd, A. D. Platt, D. Hofer, O. Ostroverkhova, M. Loth, and J. E. Anthony, "Aggregate formation and its effect on (opto)electronic properties of guest-host organic semiconductors," Appl. Phys. Lett. **97**, 163303 (2010).
24. R. R. Grollman, K. Peters, and O. Ostroverkhova, "Surface charge measurements and (dis)charging dynamics of organic semiconductors in various media using optical tweezers," Proc. SPIE **8983**, 89831N (2014).
25. M. J. Kendrick, D. H. McIntyre, and O. Ostroverkhova, "Wavelength dependence of optical tweezer trapping forces on dye-doped polystyrene microspheres," J. Opt. Soc. Am. B **26**, 2189 (2009).
26. S. H. Behrens and D. G. Grier, "The charge of glass and silica surfaces," J. Chem. Phys. **115**, 6716–6721 (2001).
27. T. Brans, F. Strubbe, C. Schreuer, S. Vandewiele, K. Neyts, and F. Beunis, "Joule heating monitoring in a microfluidic channel by observing the Brownian motion of an optically trapped microsphere," Electrophoresis **36**(17), 2102–2109 (2015).
28. W. E. B. Shepherd, A. D. Platt, G. Banton, D. Hofer, M. Loth, E. Anthony, and O. Ostroverkhova, "Effect of intermolecular interactions on charge and exciplex formation in high-performance organic semiconductors," Proc. SPIE **7935**, 79350G (2011).
29. B. M. Lowe, C. K. Skylaris, and N. G. Green, "Acid-base dissociation mechanisms and energetics at the silica-water interface: An activationless process," J. Colloid Interface Sci. **451**, 231–244 (2015).
30. J. Kim and J. H. Shin, "Stable, Free-space optical trapping and manipulation of sub-micron particles in an integrated microfluidic chip," Sci. Rep. **6**, 33842 (2016).
31. A. Kotnala, Y. Zheng, J. Fu, and W. Cheng, "Microfluidic-based high-throughput optical trapping of nanoparticles," Lab Chip **17**(12), 2125–2134 (2017).
32. R. Burger, D. Kurzbuch, R. Gorkin, G. Kijanka, M. Glynn, C. McDonagh, and J. Ducrée, "An integrated centrifugo-opto-microfluidic platform for arraying, analysis, identification and manipulation of individual cells," Lab Chip **15**(2), 378–381 (2015).
33. M. Manesse, A. F. Phillips, C. N. LaFratta, M. A. Palacios, R. B. Hayman, and D. R. Walt, "Dynamic microbead arrays for biosensing applications," Lab Chip **13**(11), 2153–2160 (2013).

1. Introduction

Processes occurring at solid-liquid interfaces are of critical importance for a variety of applications spanning diverse fields including geochemistry, environmental science, catalysis, solar energy, corrosion protection, and many others [1]. Examples of such processes include interactions involving (dis)charging of colloids [2–8], physisorption and chemisorption [9–12], (electro)chemical reactions, and photocharging [13], all of which involve evolution of the effective surface charge. In order to understand these processes, it is important to develop tools that enable systematic studies of these interactions, depending on the nature of the interface. It is also beneficial to concurrently monitor several pertinent observables, which would, for example, enable chemical identification of the surface species and of the nature of their assemblies in addition to monitoring their charge-based interaction with the environment, ideally with a possibility of enhanced spatial and time resolution [1]. Experimental platform that enables sensitive measurement of time-resolved surface charge at solid-liquid interfaces at microscopic scales, combined with spectroscopic capabilities, is the subject of the present paper.

Optics EXPRESS

Optical tweezers-based methods of measuring effective surface charge on microscopic particles suspended in polar and nonpolar liquids [2–5], [14], [15], as well as in air [16], have enabled sub-elementary charge sensitivity and time-resolved monitoring of (dis)charging processes capable of resolving single (dis)charging events [5]. Although sensitive measurements of the overall surface charge are valuable, they do not provide insight into the chemical nature of the surface and surface species interactions. Therefore, a spectroscopic component which enables simultaneous measurements of the surface charge and of specific signatures of the surface species via, for example, fluorescence or Raman spectroscopy would considerably enhance the capability of the tool and enable studies of complex environments and pertinent photoinduced interactions. In this paper, we combine a highly-sensitive method to measure surface charge on microscopic particles suspended in various environments with a capability to concurrently perform spectroscopy on the same particles, which also enables time-resolved measurements of surface charge evolution and energy transfer processes *under photoexcitation*. As an illustration, we demonstrate simultaneous surface charge and fluorescence measurement from micron-sized silica spheres coated with physisorbed fluorescent organic semiconductor molecules and their blends, suspended in different environments.

2. Materials and methods

2.1 Materials and sample preparation

Amorphous silica spheres 1 μm in diameter (Thermo Scientific, 0.99 ± 0.02 μm, refractive index n = 1.40-1.46, 2% suspension in water) were coated with diF TES-ADT or F8 TIPS-Pn molecules (Fig. 1(a), TES = (triethylsilyl)ethynyl, TIPS = (triisopropylsilyl)ethynyl) as follows. A 2 μL solution of silica spheres in water was added to 50 μL 30 mM stock solution of diF TES-ADT or F8 TIPS-Pn in toluene and sonicated for 20 minutes. Then, 14 μL of the mixture was added to 4 mL of ultra-pure millipore (Milli-Q, 18 MΩ cm) water (ε = 80), sonicated for 5 minutes, and left unperturbed overnight. As control samples, we used uncoated silica spheres, also suspended in water. Additionally, we prepared solutions of diF TES-ADT-coated silica spheres and uncoated silica spheres in toluene (ε = 2.38) following the same procedure, but replacing water with toluene at the last step of the procedure. Solutions of diF TES-ADT- coated silica spheres in a 50% wt/wt mixture of water and glycerol (ε = 64; prepared by adding 4 μL of the coated sphere solution in toluene to 4 mL of the 50% wt/wt mixture of water and glycerol) were also used as an additional control.

The ADT and Pn molecules of Fig. 1(a) are high-performance organic semiconductors [17] with well-characterized photophysics [18–21] and propensity for aggregation/crystallization when deposited from solutions on glass or silica substrates [22]. These are strongly fluorescent molecules [21] with absorption (emission) peaked at 525 nm (532 nm) and 633 nm (644 nm) for diF TES-ADT and F8 TIPS-Pn molecules, respectively, in dilute toluene solutions. Upon aggregation, both absorption and emission spectra exhibit bathochromic shifts, and their spectroscopic signatures have been studied in detail in spin-cast films [23]. These materials have also served as a model system for studies of charge and energy transfer at donor-acceptor interfaces enabled by their clear spectral signatures associated with exciplex emission and Förster resonant energy transfer, respectively [19], [20]. This prompted us to utilize such a donor-acceptor system in order to demonstrate that more complicated physisorbed layers and resulting processes can also be studied using our present approach. For this, we combined 2 mL of 30 mM diF TES-ADT (donor) and 526 μL of 2 mM diCN TIPS-ADT (acceptor) solutions [Fig. 1(a)]. After 10 minutes of sonication, 50 μL of the solution was added to a 2 μL solution of silica spheres, after which the same procedure was followed for the silica sphere coating as the one described above.

Optics EXPRESS

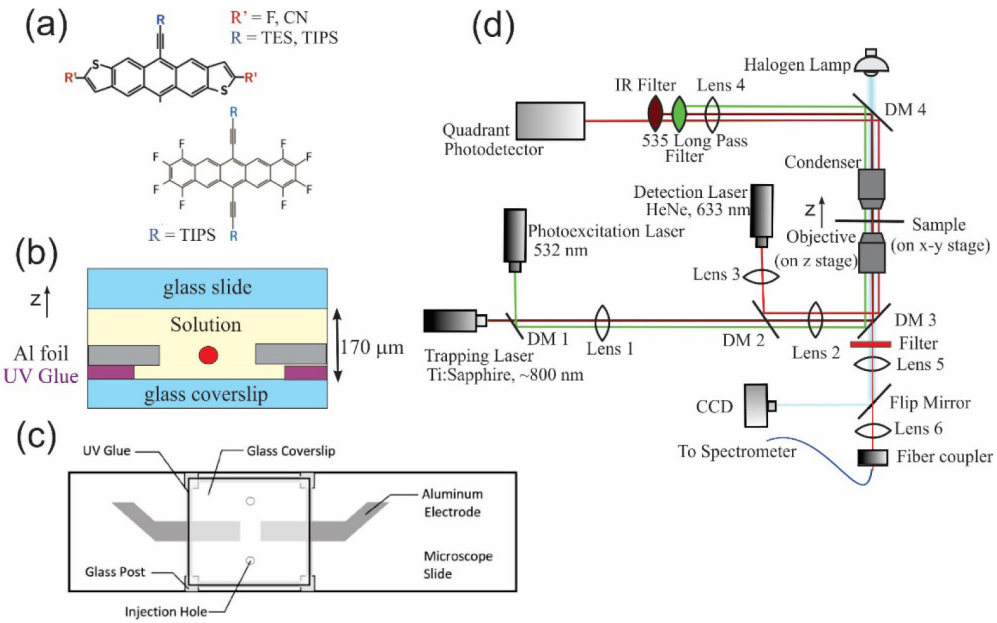

Fig. 1. (a) Molecules used for coating of the spheres: diF TES-ADT (top, R = TES, R' = F), diCN TIPS- ADT (top, R = TIPS, R' = CN), and F8 TIPS-Pn (bottom). (b) Sample holder design. The gap between Al electrodes is 100-400 µm depending on the device. The thickness of the UV glue layer is ~10 µm, the thickness of the Al foil is 24 µm, and 1 µm-diameter spheres are trapped at a depth of ~20 µm from the coverslip surface, in the middle of the gap. (c) Bottom view of the sample holder from the glass coverslip side. (d) Schematics of the experimental setup. DM = dichroic mirror. DM1 = Omega Optical 580DRLP; DM2 = Omega Optical 660DCLP; DM3 = DM4 = Edmund Optics 43955 hot mirror; Lens 1: focal length (f) f = 75 mm; Lens 2: f = 100 mm; Lens 3: f = 75 mm, placed on a x-y-z stage; Lens 4: f = 50 mm; Lens 5: f = 75 mm; Lens 6: f = 100 mm; 535 Long Pass filter = Chroma Tech HQ535LP; IR filter = Thorlabs FES0650. Filter in front of Lens 5 is either a long-pass 532 nm (Edmund Optics RazorEdge 532 LP) or a 632.8 nm notch (Edmund Optics 63-347 632.8 OD6 Notch Filter), depending on the coating. Fiber coupler = Siskiyou RM80-1; CCD = Marshall V-1050A; Spectrometer = Ocean Optics USB2000-FLG.

Solutions of either uncoated or coated silica spheres were inserted into a sample holder with coplanar Al electrodes shown in Fig. 1(b). A sample holder [24] consists of a 22 x 22 x 0.17 mm glass coverslip (Fisher Scientific, 12-541-B) and 25 x 75 x 1 mm glass microscope slide (VWR, 48300-026). Two holes are drilled in the glass microscope slide [Fig. 1(c)] using a diamond-tip dremel tool to allow for injection of the solution with suspended particles under study; after drilling the slide is rinsed with toluene and deionized water to remove all glass particles from the surface. The glass coverslip and microscope slide are assembled using four 5 x 5 mm squares cut out from another glass coverslip as spacers which are attached with the UV glue (Thorlabs, NOA81) to the glass microscope slide [Fig. 1(c)] and cured under a UV lamp for 45 seconds. Two strips (5 mm x 60 mm) are cut out from heavy-duty Al foil (Reynolds Wrap) and attached to the center of a coverslip with the UV glue (cured under the UV lamp for 45 seconds), leaving a 70-400 µm gap, to serve as Al electrodes. Lastly, the edges of the coverslip are lines with the UV glue, creating a sealed chamber, and the finished holder is cured under the UV lamp for 60 seconds. The solution containing spheres under study suspended in a solvent of choice is injected through the holes into the chamber immediately before the experiments.

Optics EXPRESS

2.2 Setup combining optical tweezers and spectroscopy capability

Optical tweezer trapping was performed in a custom inverted microscope assembly with an oil immersion microscope objective (Edmund Optics, 100X, NA of 1.25, 160 mm tube length) as shown in Fig. 1(d) [25]. Spheres were trapped with a continuous wave (cw) 800 nm Ti:Sapphire laser beam (KM Labs, Inc.). The position of the trapped sphere was detected by the scattering of a cw 633 nm Helium-Neon laser detected by a Hamamatsu S4349 quadrant photodetector (QPD). The QPD signal was collected using a data acquisition card (DAQ) (NI-6221) at 10 or 20 kHz read out by a custom LabVIEW program. The duration of each position versus time measurement (x(t)) was 25-30 s. Spheres were trapped in the center of the electrode gap to minimize edge effects, and at a depth of about 20 μm away from the top of the coverslip to minimize interactions between the sphere and the glass slide [2], [26].

Additionally, a cw 532 nm (Coherent, Inc. Verdi-5) laser beam, collimated to minimize its effect on the trap stability, was used to excite spheres coated with diF TES-ADT or diF TES-ADT:diCN TIPS-ADT blend. Spheres were imaged with a CCD and halogen lamp. Filters were placed in front of the QPD to block the 800 nm and 532 nm light. For spheres coated with F8 TIPS-Pn, which was more efficiently excited at 633 nm than at 532 nm, the role of the 633 nm and 532 nm beams was reversed, and a filter in front of the QPD was replaced with a band-pass filter to block the 633 nm excitation while passing scattering of the 532 nm light. In each case, fluorescence spectra from the trapped spheres, examples of which are shown in Fig. 2, were measured using a fiber-coupled Ocean Optics USB2000-FLG spectrometer. No fluorescence was observed from uncoated silica spheres.

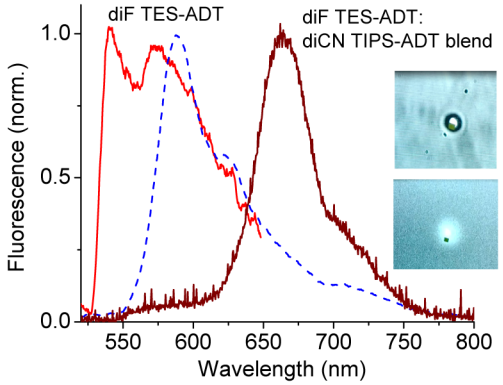

Fig. 2. Fluorescence from trapped silica spheres coated with diF TES-ADT and with diF TES-ADT:diCN TIPS-ADT blend suspended in water. In the spectrum of the diF TES-ADT-coated sphere, the ~540 nm peak is due to isolated molecules, whereas the ~580 nm peak is due to diF TES-ADT aggregates. Spectrum from a micron-sized diF TES-ADT aggregate suspended in water is also included (dashed line). The spectrum from the blend is dominated by the ~670 nm peak due to the diF TES-ADT: diCN TIPS-ADT exciplex formation. Inset shows CCD images of a trapped diF TES-ADT-coated sphere in water without (top) and with (bottom) 532 nm photoexcitation, illustrating strong diF TES-ADT fluorescence under photoexcitation.

2.3 Trap stiffness and effective charge measurement

The trap stiffness in the x-y plane and the effective surface charge were calculated from the power spectrum of the suppressed Brownian motion of the sphere x(t) [Fig. 3(a)] [25]. In particular, in the presence of the applied sinusoidal (AC) electric field, the power spectrum of the position fluctuations (Fig. 3(b)) is given by

$$\left|\tilde{x}(f)\right|^2 = \frac{k_B T}{\pi^2 \beta (f_c^{\,2} + f^2)} + \frac{k_B T \gamma^2}{k} \delta(f - f_{AC}). \qquad (1)$$

Optics EXPRESS

Here k_B is the Boltzmann constant, T is the temperature, f is the frequency, β is the drag coefficient of the sphere in the medium ($\beta = 6\pi R\eta$, where R is the radius of the sphere and η is the dynamic viscosity), f_c is the corner frequency, and f_{AC} is the frequency of AC electric field. The corner frequency is related to the trap stiffness (k) as $f_c = k/(2\pi\beta)$, from which the trap stiffness k is readily obtained. The trap stiffness was in the range of 1-2 pN/μm for all samples. The constant γ^2 is the scaled ratio of the mean-square periodic and Brownian forces given by [2]

$$\gamma^2 = \frac{e^2 Z_{eff}{}^2 E^2}{2k_B T k} \frac{1}{1+(f_{AC}/f_c)^2}. \quad (2)$$

From the experimental data, the γ^2 was extracted by integrating the power spectrum component due to applied electric field (second term of Eq. (1)) with respect to frequencies [2], [3] and the integral is $P_{AC} = k_B T \gamma^2 / k$. Then, the effective charge Z_{eff} on a sphere was calculated using [2]

$$eZ_{eff} = \frac{\gamma\beta}{E}\sqrt{\frac{2k_B T}{k}((2\pi f_{AC})^2 + (k/\beta)^2)}, \quad (3)$$

where e is the charge of an electron and E is the applied electric field. The sign of the charge was determined by following the oscillatory motion of the free particle at low f_{AC} while briefly blocking the trapping laser beam thus momentarily releasing the particle from the trap [2].

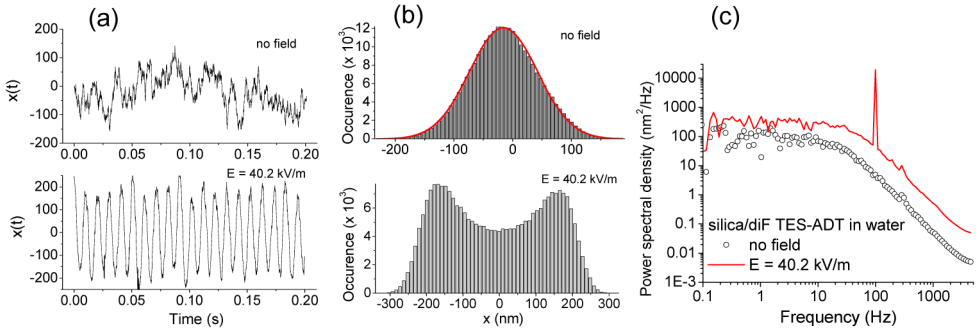

Fig. 3. (a) Time-dependent position of a trapped sphere (x(t)) in the absence (top) and in the presence (bottom) of AC electric field (E = 40.2 kV/m) for a silica sphere coated with diF TES-ADT in water. (b) Histograms of the particle position of (a) without (top) and with (bottom) electric field. (c) Power spectral density obtained from data in (a) showing appearance of the peak due to charge moving in the applied AC electric field with f_{AC} = 98 Hz. The corner frequency f_c for both data sets is 25 Hz. The data were offset along y-axis for clarity.

An AC voltage of 0.5 V_{pp} to 20 V_{pp} was applied across electrodes using an amplified sinusoidal signal from a function generator (Tektronix AFG3021) and the range of frequencies f_{AC} between 10 Hz and 4 kHz. In devices using toluene as the medium, the electric field E was calculated as $E = \lambda V_0/d$ where V_0 is the voltage amplitude and d is the distance between the electrodes. The scaling factor λ takes into account the electric field dependence on the position of the sphere with respect to the coplanar electrodes [2] and is in the range between 0.9 and 0.95, depending on the device. In water-based devices, the presence of an electric double layer, formed as a result of ion accumulation at the electrodes, was detected. This resulted in a frequency-dependent electric field $E(f_{AC})$ that approaches $\lambda V_0/d$ at high frequencies but is partially screened at low frequencies f_{AC} [3]. Following Ref

Optics EXPRESS

[3], such dependence was obtained from modeling the devices using an equivalent circuit approach with a frequency-dependent impedance so that $E(f_{AC}) = (\lambda V_0/d)\, R_b/Z(f_{AC})$ where

$$Z(f_{AC}) = R_b - \frac{i}{2\pi f_{AC} C_b} + R_{dl}\frac{1 - i2\pi f_{AC} R_{dl} C_{dl}}{1 + (2\pi f_{AC} R_{dl} C_{dl})^2}. \quad (4)$$

Here R_b and C_b are resistance and capacitance of the bulk and R_{dl} and C_{dl} are those of the double layer [3].

No considerable changes in the trapping stiffness k or the effective charge Z_{eff} were observed upon the 532 nm photoexcitation at least up to a power of 28 mW, which is considerably higher than typical powers of <5 mW which were used for photoexcitation. This indicates that the charge and fluorescence measurements can be performed simultaneously, without perturbing the system.

2.4 Time-dependent effective charge measurement

In addition to the effective charge measurement using the power spectrum of Fig. 3(c) as described above, we explored an alternative method of obtaining the effective charge from the data, more suitable for achieving enhanced time resolution of the measurement [5], [16]. In the presence of applied AC electric field, the particle displacement x(t) can be presented as a sum of two contributions, the displacement due to random thermal forces ($x_n(t)$) and that due to periodic forces ($x_p(t)$) [2]. At high electric fields, the latter dominates, the trend for which can be appreciated from comparison between the x(t) data in Fig. 3(a) and 3(b) (top *vs* bottom). In that case, x(t) is dominated by $x_p(t)$, and the amplitude of the sinusoidal displacement x_0 can be related to the effective charge as follows [2]:

$$x_0 = \frac{eZ_{eff}E}{k\sqrt{1 + (f_{AC}/f_c)^2}}. \quad (5)$$

This method provides the time resolution determined by the AC field frequency, and the sampling frequency at which the charge is estimated ($f_{s,Q}$) can be varied ($f_{s,Q} < f_{AC}$) to achieve averaging of the extracted charge values over a specified time window [4]. In our time-resolved experiments, we used f_{AC} = 100 Hz and time window durations ranging from 250 ms ($f_{s,Q}$ = 4 Hz) to 8.3 ms ($f_{s,Q}$ = 120 Hz).

3. Results and discussion

Figure 4(a) shows dependence of the parameter γ^2 of Eq. (1) on the frequency of applied electric field f_{AC}. While toluene-based devices exhibited frequency dependence expected based on Eq. (2) [inset of Fig. 4(a)], water-based devices showed a more complicated pattern [Fig. 4(a)]. The latter behavior has been previously attributed to the formation of the double layer at the electrodes and a resulting frequency dependence of the amplitude of the AC electric field (E in Eq. (2)) via Eq. (4) that contributes to the overall frequency dependence of γ^2 by modifying a low-frequency response. The fit of the data in Fig. 4(a) to the model (Sec. 2.3) [3] with R_b = 80 kΩ, C_b = 0.01 μF, R_{dl} = 300 kΩ, and C_{dl} = 0.4 μF of Eq. (4) is also included in the figure. With these parameters, the amplitude of the electric field is an increasing function of f_{AC} exhibiting values of ~0.44 E_0 at 100 Hz, 0.7 E_0 at 200 Hz, 0.93 E_0 at 500 Hz, and > 0.98 E_0 at ≥ 1kHz where E_0 is the maximal field amplitude ($E_0 = \lambda V_0/d$).

Figure 4(b) shows dependence of γ on the amplitude of applied electric field E at f_{AC} of 110 Hz. Linear response was observed in all devices, in agreement with expectations based on Eq. (2). This confirms that the charge on particles is independent of the strength of the applied field, regardless of the coating or of the surrounding medium. The trap stiffness was also not affected by electric field [Fig. 3(c)], confirming no appreciable field-induced heating [27]. The limiting charge sensitivity, determined by the minimal detectable value γ distinguishable

Optics EXPRESS

from the noise due to the Brownian motion at f_{AC}, was ~3e at 10 kV/m and ~0.3e at 100 kV/m, comparable to that achieved in previous studies [2].

Figure 5 shows distributions of absolute values of effective charge density ($|Z_{eff}|/4\pi R^2$, where R = 500 nm is the radius of the sphere) obtained in various systems under study using the method described in Sec. 2.3. In all systems, only negative Z_{eff} charge values were observed. The width of distributions represents a spread in values obtained from various spheres of the same type suspended in the same liquid, across different devices. Each value of charge density in the histogram is an average over at least 4 experimental runs for an individual sphere, and the run-to-run error for each given sphere is less than 5%.

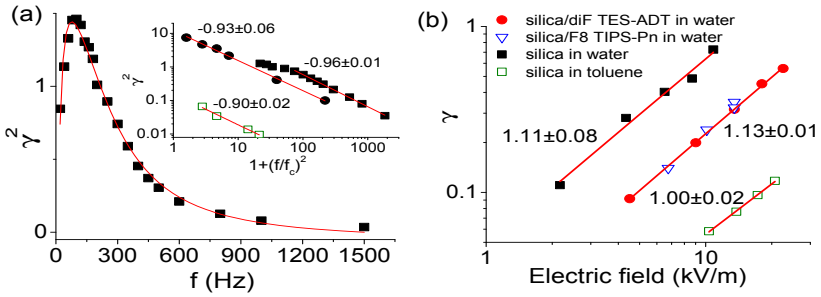

Fig. 4. (a) Frequency dependence of the parameter γ^2 of Eq. (1) obtained from a silica sphere in water. Fit to the model of Eq. (2) with frequency-dependent electric field (Eq. (4)) is also included. Inset shows higher frequency behavior of two silica spheres in water (solid squares and circles) and of a silica sphere in toluene (open squares). The linear fits show a slope close to −1 in all cases, in accordance with Eq. (2). (b) Electric field dependence of γ obtained from coated and uncoated silica spheres. Linear fits show a slope close to 1, in accordance with Eq. (2).

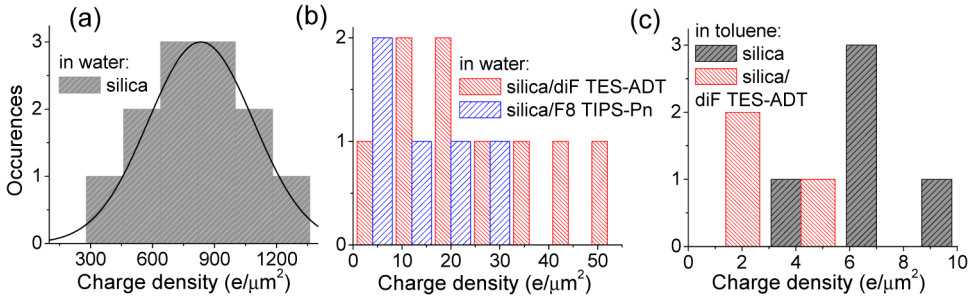

Fig. 5. Absolute values of charge densities obtained from various systems, in particular: uncoated silica spheres in water (a), silica spheres coated with diF TES-ADT or F8 TIPS-Pn in water (b), and silica spheres, uncoated and coated with diF TES-ADT, in toluene (c).

The distribution obtained from uncoated silica spheres in water was fit with a Gaussian function (~$\exp(Q-Q_{max})^2/2\sigma^2$, where Q is the charge density and σ is the standard deviation) revealing the peak (Q_{max}) at −830 ± 30 e/μm^2, comparable to previously reported values in a similar system [26]. The negative effective charge on silica spheres in water is due to the dissociation of the silanol groups ($SiOH \leftrightarrow SiO^- + H^+$), which gives rise to the surface charge density $\sigma_s = -e\Gamma_{SiO^-}$, where e is the elementary charge and Γ_{SiO^-} is the density of dissociated groups [26]. In coated spheres suspended in water, the charge density was more than an order of magnitude lower, ranging between −4 e/μm^2 and −50 e/μm^2 [Fig. 5(b)], depending on the quality of the coating as discussed below. As the neutral, hydrophobic functionalized ADT and Pn molecules of Fig. 1(c) do not undergo charge species-producing chemical reactions with water, the dramatic reduction in the surface charge density indicates efficient prevention of the silica-water interaction due to the organic semiconductor layer adsorbed on the silica surface that reduces the number of reaction sites. As expected, further reduction in charge

Optics EXPRESS

densities (down to fewer than −5 $e/\mu m^2$) was observed in the coated spheres suspended in the water/glycerol mixture.

Fluorescence spectra obtained from coated trapped spheres [Fig. 2] enable evaluation of the molecular packing and interactions in the adsorbed organic semiconductor layer. For example, the spectrum for a diF TES-ADT coated sphere obtained at 532 nm excitation in Fig. 2 illustrates an interplay of the diF TES-ADT monomeric (peaked at ~540 nm) and aggregate (peaked at ~580 nm) emission, with the latter dominating spectra of coatings with better surface coverage and producing lower effective charge densities in the distribution of Fig. 5(b). For comparison, the spectrum from a micron-sized diF TES-ADT aggregate in water measured using the same experimental setup is also included in Fig. 2, showing exclusively aggregate emission as well as self-absorption effects. Evolution of spectra from monomeric to aggregate-dominated emission in diF TES-ADT, as well as self-absorption effects, has been previously studied in diF TES-ADT:PMMA films (PMMA = poly(methyl methacrylate)) spin cast or drop cast on glass substrates, depending on the diF TES-ADT concentration and film thickness [23], [28], and is consistent with current observations from various diF TES-ADT-coated spheres. Additionally, fluorescence spectra obtained from trapped spheres coated with a diF TES-ADT:diF TES-ADT:diCN TIPS-ADT blend were similar to those obtained from spin-cast thin films of these materials [19]. In particular, they are characteristic of the diF TES-ADT:diCN TIPS-ADT exciplex that forms at the interface between the diF TES-ADT donor and diCN TIPS-ADT acceptor as a result of a partial donor-acceptor charge transfer [19], [20] that quenches the diF TES-ADT donor emission thus dominating the spectrum of the blend. This suggests that studies of more complicated physisorption processes and of resulting photophysics and charge-based interactions are also possible with this technique.

In toluene, charge densities peaked at about −7 $e/\mu m^2$ on uncoated silica and were further reduced in coated spheres [Fig. 5(c)]. The mechanism of charging of silica in nonpolar medium such as toluene is not well understood; it is hypothesized that it is similar to that in water, but having less frequent charging events due to the stronger electrostatic interaction between charges [4]. Effective charge Z_{eff} ranging between −12e and + 10e was previously observed on 1 μm silica spheres suspended in dodecane using optical tweezer-based measurements [4], and charge between −70e and + 20e was observed in electrophoretic measurements of silica particles in dodecane. Observation of the charge on silica in nonpolar dodecane that is more than two orders of magnitude lower than that on silica in water [4] is similar to our observations in silica spheres in nonpolar toluene *vs* water in Figs. 5(c) and 5(a), respectively. Further decrease in the charge density observed in coated spheres suspended in toluene [Fig. 5(c)] is consistent with the hypothesis of the same charging mechanism for silica spheres in toluene as that in water, such that the coating reduces the number of reaction sites on a silica sphere.

Next, we evaluated the potential for the time-resolved charge measurements using the amplitude of the field-driven sphere x_0 of Eq. (5) and a method described in Sec. 2.4. The relative accuracy of this method with respect to that of Sec. 2.3 (that relies on the power spectrum analysis) depends on the applied electric field amplitude E and the frequency f_{AC} with respect to the corner frequency f_c [Eq. (5)]. We found that at E = 9.2 kV/m, f_{AC} = 100 Hz, f_c = 40 Hz, and averaging time window of 25 s the effective charge (Z_{eff}) on a silica sphere in water obtained with the method relying on x_0 was within 2% of the value derived using the power spectrum obtained from the same x(t) data. Then, we proceeded to use these data and split the time window of 25 s into non-overlapping windows of either 250 ms ($f_{s,Q}$ = 4 Hz) or 10 ms ($f_{s,Q}$ = 100 Hz) calculating the Z_{eff} values from the x_0 values averaged over each window. Figure 6(a) shows the effective charge density ($|Z_{eff}|/4\pi R^2$) as a function of time obtained in these two cases; the window-to-window distributions of these values, along with Gaussian fits, are shown in the inset. A factor of 25 increase in the averaging time reduced the time-dependent charge fluctuations [here quantified by $2\sigma/Q_{max}$, where Q_{max} is the peak value

Optics EXPRESS

of the charge density and σ is the standard deviation, both obtained from the Gaussian fits to the data in Fig. 6(b)] from ~20% to ~5%. In the presence of processes involving time-varying effective surface charge, such as adsorption, these distributions are expected to shift (e.g. to the lower Q_{max} values in the case of adsorption of organic molecules used here), which can be measured as a function of time with a time resolution determined by the amount of the change in effective charge to be monitored.

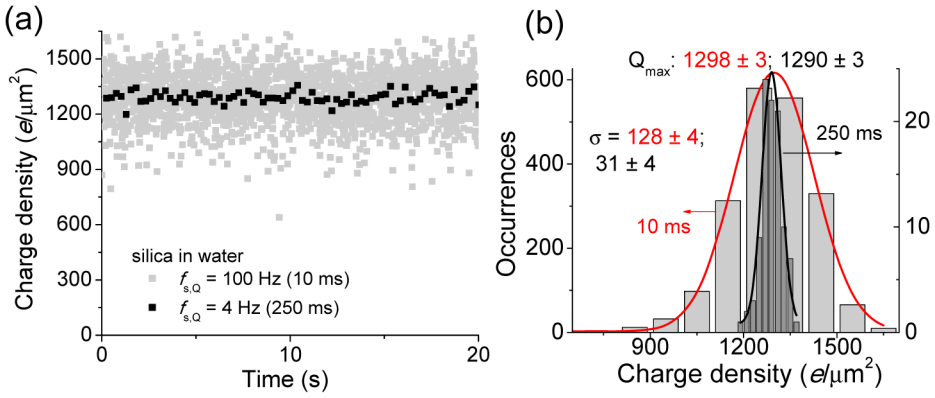

Fig. 6. (a) Charge density fluctuations in time on a silica sphere in water. Each data point corresponds to charge density averaged over a 250 ms time window (black squares) or a 10 ms time window (grey squares). (b) Distribution of obtained effective charge density values of (a) for 250 ms windows (right axis) and 10 ms window (left axis). Gaussian fits and the peak charge density values (Q_{max}) and standard deviations (σ) obtained from the fits are also shown.

The trade-off between time and charge resolution clearly observable in Fig. 6(b) can also be appreciated from the condition $eE / \sqrt{4k_B T \beta f_{s,Q}} > 1$ which needs to be satisfied in order to achieve single charge resolution [5]. With experimental parameters used for obtaining data in Fig. 6 (T = 297 K, β = 8.4 nN s/m, E = 9.2 kV/m, f_{AC} = 100 Hz, and f_c = 40 Hz) the left-hand-side yields only ~0.064 for $f_{s,Q}$ = 4 Hz. Thus, the condition is not satisfied, and a factor of >15 higher electric fields (E), a factor of >245 lower sampling frequency $f_{s,Q}$ (corresponding to several tens of seconds in time resolution), or a combination of both factors, would be necessary for single-charge resolution.

Previous time-resolved studies of effective surface charge on optical tweezers-trapped polymer microspheres suspended in nonpolar liquids have achieved single charge resolution at high electric fields (on the order of MV/m). Discrete (dis)charging events were observed, which was enabled by slow charge exchange of one electron per second, thus not requiring high sampling frequencies $f_{s,Q}$ (as $f_{s,Q}$ should be considerably higher than the frequency at which such events occur to achieve single-charge resolution) [4], [5]. In polar media, charge exchanges are considerably faster, and such detection has not yet been achieved; using even higher electric fields and high frequencies, as well as smaller particles, has been suggested as a potential solution. The time-resolved monitoring of silanol dissociation in water (which is the source of the surface charge on silica spheres) with a single-charge resolution would require sub-picosecond time resolution [29] and is not achievable with a current technique. However, such monitoring of slow processes such as diffusion-limited interactions of the sphere coating with molecular or ionic species introduced in the environment, as well as evolving interactions between the molecular species at the surface, are readily accessible.

The spectroscopic capability complements the effective charge measurement by introducing concurrent monitoring various light-induced processes and enables chemical identification of the adsorbed layers. The processes are not limited to fluorescence from the adsorbed molecules (used here as an illustration), but include photoinduced charge and energy transfer between the molecules in the coating and in the environment, charge-

Optics EXPRESS

dependent Raman shifts, (dis)charging under photoexcitation, etc. The measurements can also be performed on particles trapped in microreactors and microfluidic channels [15] using a continuous flow channel design [30], [31] instead of a non-refillable sample chamber used in our studies, and with multiplexed detection [30], [32], [33], which further extends the range of possible applications.

4. Conclusions

Experimental platform which combines spectroscopic capabilities with time-resolved measurements of effective surface charge at solid-liquid interfaces is presented. Adsorption of organic semiconductor molecules on micron-sized silica spheres was observed via appearance of fluorescence and up to two orders of magnitude reduction in the effective surface charge, measured concurrently on individual spheres, optically trapped in different environments, with elementary charge resolution. The platform accommodates possibilities to measure various photoinduced processes concurrently with measurements of surface charge and can be further extended to in situ monitoring of time-varying charge- and energy exchange in devices such as microreactors and microfluidics.

Funding

National Science Foundation (NSF) (DMR-1207309); Oregon State University (URISC program)

Acknowledgments

We thank Prof. J. E. Anthony for diF TES-ADT, diCN TIPS-ADT, and F8 TIPS-Pn derivatives. Contributions of Prof. D. McIntyre, Dr. M. Kendrick, K. Peters, and J. Busche to the early developments of this project are gratefully acknowledged.